Supporting Information Appendix for

Efficient Water Oxidation Catalyzed by Cationic Cobalt Porphyrins: Critical Roles for the Buffer Base

Dong Wang and John T. Groves*

Department of Chemistry, Princeton University, Princeton, NJ 08544

Materials and Methods

All chemicals are of the highest commercially available purity and were used as received, unless noted otherwise. Water used in all experiments was distilled and deionized by a Milli-Q system from Millipore. TDMImP was synthesized according to reported procedures (1). TM4PyP and TTMAP were purchased from Frontier Scientific, Inc. Co- and Ga-porphyrins were synthesized by metalating the corresponding porphyrin free base with cobalt(II) acetate or gallium(III) chloride respectively in H_2O (2) and purified as the chloride salt by a double-precipitation method (3).

UV-vis spectra were recorded with a Hewlett-Packard 8453 diode array spectrometer at room temperature. CV, SWV and controlled potential bulk electrolysis were performed on a BAS 100B electrochemical workstation in pH buffered aqueous solutions at room temperature using a Ag/AgCl reference electrode, a glassy carbon or indium tin oxide (ITO, resistance 10 Ohm per square inch, Nanocs) working electrode, and a Pt auxiliary electrode. pH was measured using an accumet AB15 pH electrode from Fisher Scientific. O_2 evolution was measured by a YSI 550A Clark electrode from Fondriest Environmental. ESEM and EDX analysis were carried out on a Quanta 200 FEG ESEM. Details about fitting the buffer concentration effect on water oxidation catalysis are described below.

Data fitting.

Electrocatalytic equation:

$i_{cat} = nFAD_{cat}^{1/2}C_{cat}k_{cat}^{1/2}$; $k_{cat} = k_{water} + k_b[B]$

$$(i_{cat}/i_{water})^2 = (C_{cat}/C_{cat}^{o})^2(k_{cat}/k_{water}) = (C_{cat}/C_{cat}^{o})^2(1 + k_b[B]/k_{water}) \quad (S1)$$

i_{cat}: overall catalytic current

i_{water}: current without the presence of buffer base

n: number of electrons transferred

F: Faraday constant

A: surface area of the working electrode

C_{cat}: effective concentration of active catalyst

C_{cat}^{o}: total concentration of catalyst

D_{cat}: diffusion coefficient of catalyst

k_{cat}: overall rate constant of the O-O bond formation (pseudo-first-order)

k_{water}: rate constant of the O-O bond formation in unbuffered solution (pseudo-first-order)

k_b: rate constant of the O-O bond formation contributed by the addition of buffer base (second order)

For an inhibition pathway that involves the following equilibria:

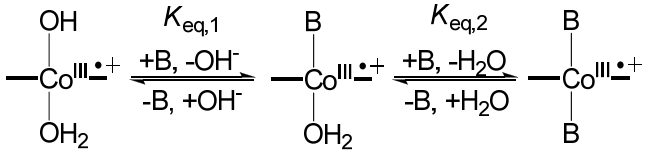

$K_{eq,1} = [Co^{III}\text{-}B][OH^-]/[Co^{III}\text{-}OH][B]$; $K_{eq,2} = [Co^{III}\text{-}B_2][H_2O]/[Co^{III}\text{-}B][B]$

So, $[Co^{III}\text{-}B] = K_{eq,1}[Co^{III}\text{-}OH][B]/[OH^-]$

$[Co^{III}\text{-}B_2] = K_{eq,2}[Co^{III}\text{-}B][B]/[H_2O] = K_{eq,1}K_{eq,2}[Co^{III}\text{-}OH][B]^2/[OH^-][H_2O]$

Mass balance: $[Co^{III}\text{-}OH] + [Co^{III}\text{-}B] + [Co^{III}\text{-}B_2] = [Co^{III}\text{-}OH]^o$

$C_{cat}/C_{cat}^{o} = [Co^{III}\text{-}OH]/[Co^{III}\text{-}OH]^o = 1/(1 + K_{eq,1}[B]/[OH^-] + K_{eq,1}K_{eq,2}[B]^2/[OH^-][H_2O])$ (S2)

Combine eqs S1 and S2:

$(i_{cat}/i_{water})^2 = (1 + k_b[B]/k_{water})/(1 + K_{eq,1}[B]/[OH^-] + K_{eq,1}K_{eq,2}[B]^2/[OH^-][H_2O])^2$ (S3)

For an aqueous solution buffered at pH 7, $[OH^-] = 10^{-7}$ M, $[H_2O] = 55.6$ M

At low buffer concentration,

$1 + K_{eq,1}[B]/[OH^-] + K_{eq,1}K_{eq,2}[B]^2/[OH^-][H_2O] \approx 1$

Eq S3 then becomes: $(i_{cat}/i_{water})^2 = 1 + k_b[B]/k_{water}$, the same as eq. 4 in the text.

Fits of concentration dependence of catalytic current for four buffers used, as shown in Figure S18, were obtained using eq. S3. Fitted parameters (k_b/k_{water}, $K_{eq,1}$, and $K_{eq,1}K_{eq,2}$) are summarized in Table S1.

Table S1. Summary of parameters obtained from fittings according to eq. S3.

Buffer	Phthalate	Na-Pi	*n*-BuPi	*t*-BuPi
$K_{eq,1}$	2.7E-7	4.3E-7	1.7E-6	6.8E-6
$K_{eq,2}K_{eq,1}$	1.6E-5	2.1E-4	4.8E-3	3.4E-2
k_b/k_{water}	500	2400	2650	4510
R^2	0.99	0.90	0.99	0.99

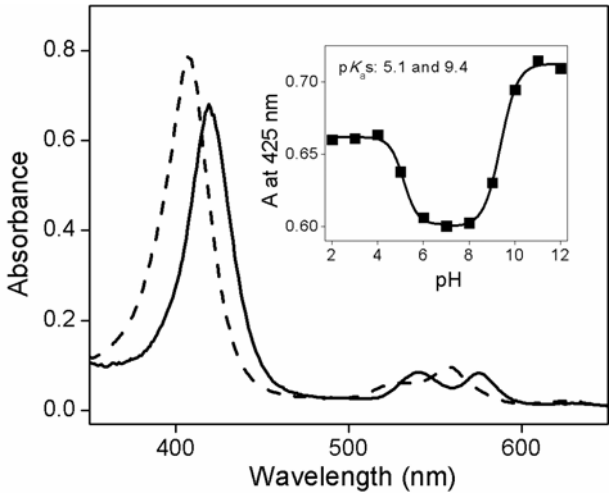

Figure S1. Optical spectra of 10 μM Co-TDMImP in the form of $Co^{II}(OH_2)_2$ (λ_{max} = 407, 527, 558 nm) (dashed) and $Co^{III}(OH)(OH_2)$ (λ_{max} = 419, 540, 575 nm) (solid) at pH 7. Species not shown: $Co^{III}(OH_2)_2$ at pH 2 (λ_{max} = 420, 539, 575 nm) and $Co^{III}(OH)_2$ at pH 12 (λ_{max} = 425, 545, 579 nm). Inset: pH titration curve of Co^{III}-TDMImP monitored at 425 nm. The two pK_a values were derived from data fitting.

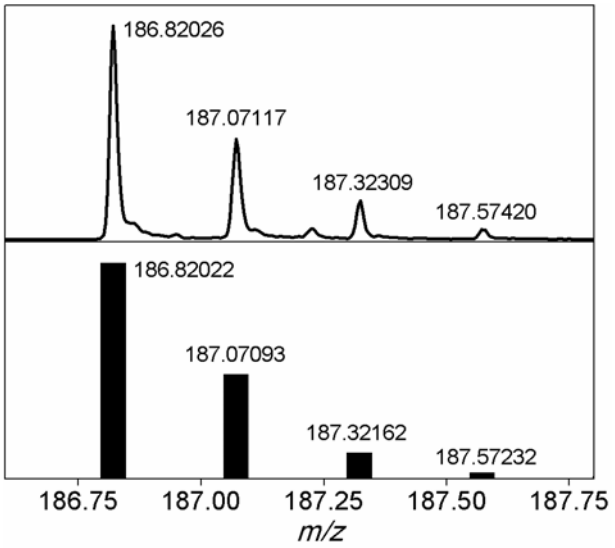

Figure S2. Experimental (top) and simulated (bottom) ESI-MS spectra of $[Co^{II}$-TDMImP$]^{4+}$. Precise *m/z* values are listed next to each peak.

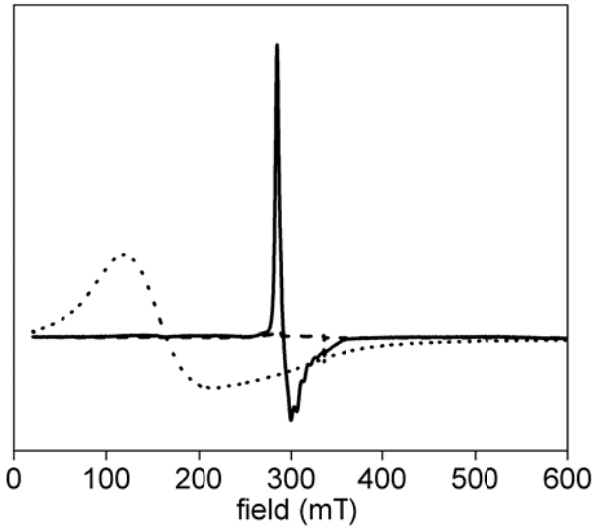

Figure S3. CW X-band EPR spectra of frozen samples in water of 1 mM Co(acetate)$_2$ (dotted, g_{eff} = 5.56 and 3.13), 1 mM Co^{II}-TDMImP (solid, g_{eff} = 2.30), and 1 mM Co^{III}-TDMImP (dashed, EPR silent). T = 5 K; microwave power = 0.2 mW.

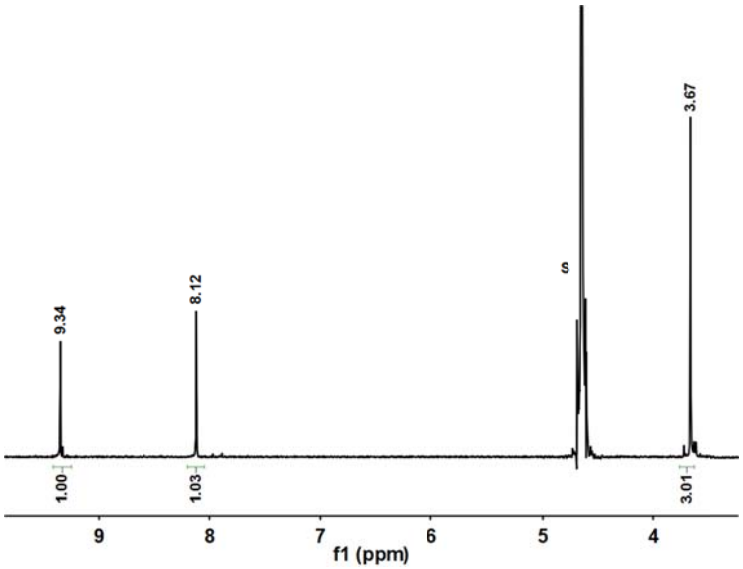

Figure S4. ^{1}H NMR spectrum of 1 mM Co^{III}-TDMImP obtained in D_2O. Chemical shifts are labeled above each peak: δ 9.34 (s, porphyrin β-pyrrole-H, 8H), 8.12 (s, imidazolium-H, 8H), 3.67 (s, methyl-H, 24H).

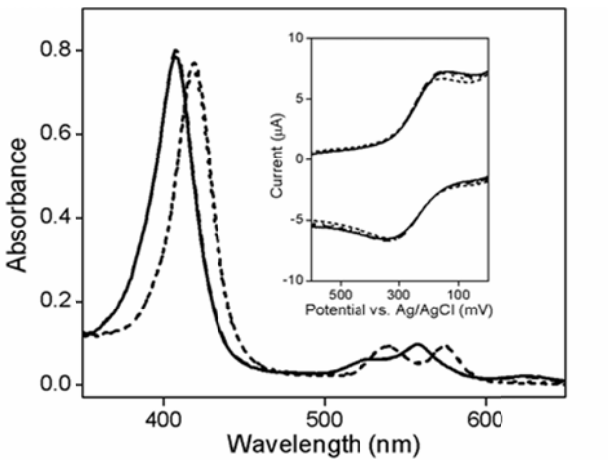

Figure S5. Optical spectra recorded at room temperature of 10 μM Co^{II}-TDMImP in unbuffered H_2O (solid) and 1 M Na-Pi buffer at pH 7 (dashed), and 10 μM Co^{III}-TDMImP in unbuffered H_2O (dotted) and 1 M Na-Pi buffer at pH 7 (short dashed). Inset: CVs of 1 mM Co-TDMImP at room temperature and a scan rate of 100 mV s^{-1} in pH 7 solutions containing Na-Pi buffer of 0.01 M (solid), 0.05 M (dashed), 0.1 M (dotted), and 0.2 M (short dashed) at room temperature.

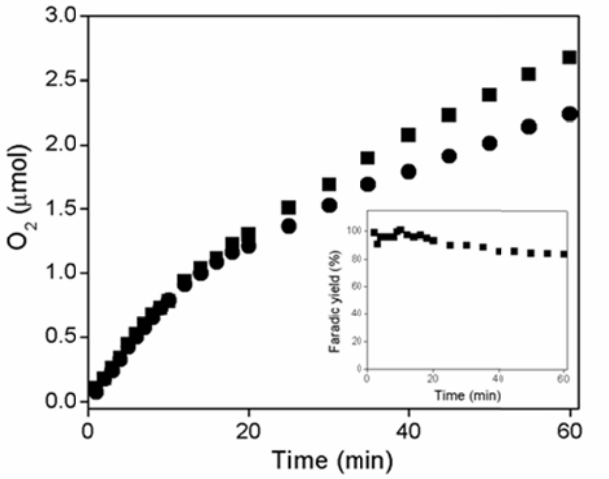

Figure S6. Theoretical (filled squares) and measured (filled cycles) O_2 formation (in μmol) during controlled potential electrolysis of 0.5 mM Co-TDMImP for 1 h at 1300 mV in 0.2 M Na-Pi buffer at pH 7. Inset: plot of the O_2 formation yield as a function of time.

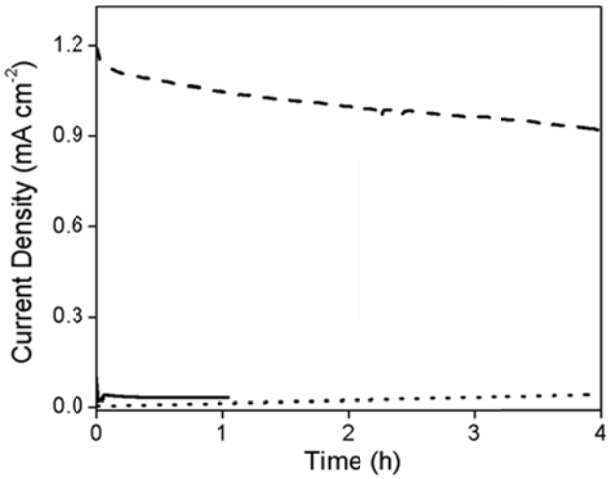

Figure S7. Current density profile of controlled potential bulk electrolysis of buffer background (dotted); 0.5 mM Co-TDMImP solution (dashed); and clean buffer using the same ITO working electrode after the red trace was obtained (solid). Other conditions: room temperature, 0.2 M Na-Pi buffer at pH 7, applied potential 1300 mV.

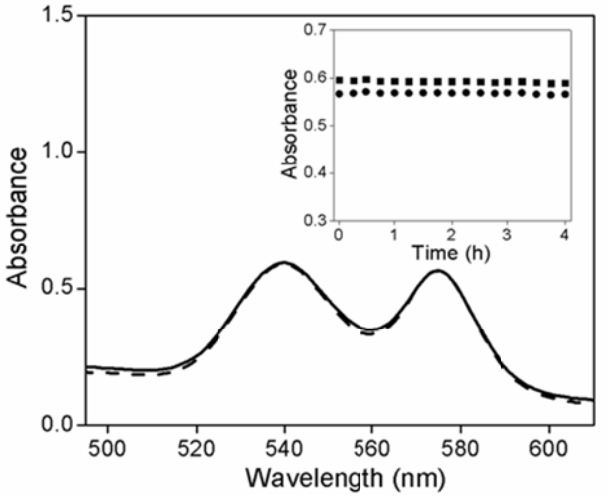

Figure S8. UV-vis spectra of 0.5 mM Co^{III}-TDMImP before (solid) and after (dashed) electrolysis at an applied potential of 1300 mV for 4 hours. Inset: plot of the absorption maximum of the two Q-bands at 540 nm (filled squares) and 575 nm (filled circles) as a function of time.

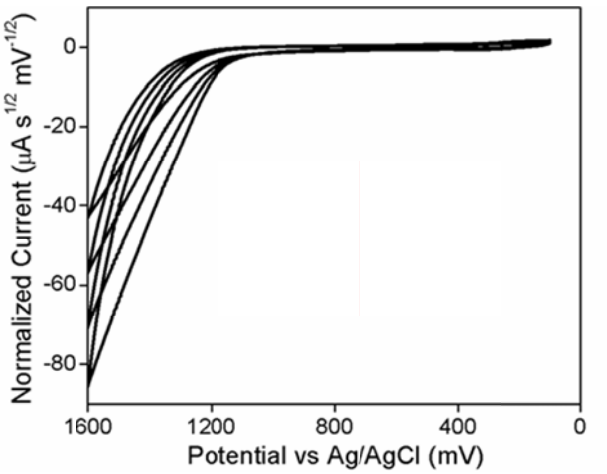

Figure S9. CVs of 1 mM Co-TDMImP at room temperature in 0.2 M Na-Pi buffer at pH 7 showing the current normalized on the basis of the square root of scan rate at a scan rate of (from top to bottom) 500 mV s^{-1}, 200 mV s^{-1}, 100 mV s^{-1}, and 50 mV s^{-1}.

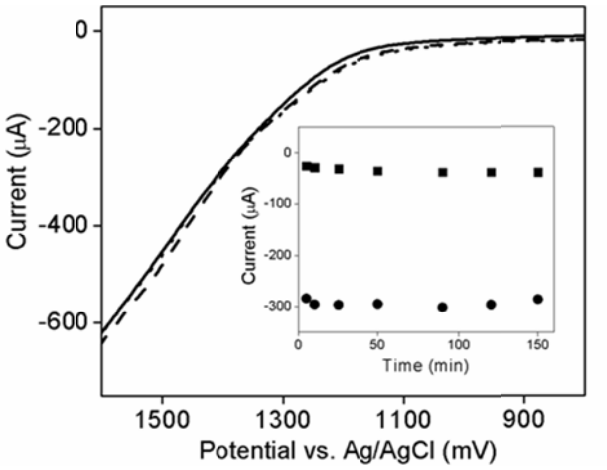

Figure S10. Linear sweep voltammetry of 1 mM Co-TDMImP in 0.2 M Na-Pi buffer at pH 7 monitored for the first 150 minutes after the solution was freshly prepared. Showing are scans taken at 5 (solid), 50 (dashed) and 150 (dotted) minutes. Inset: plot of current at 1100 mV (filled squares) and 1400 mV (filled circles) as a function of time.

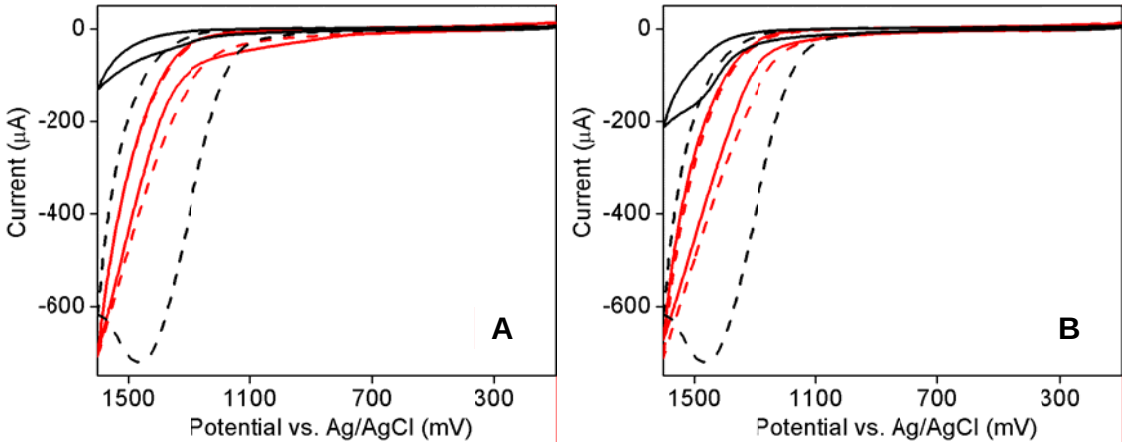

Figure S11. (A) CVs of 1 mM Co-TDMImP (red) and 0.2 mM $Co(NO_3)_2$ (black) before (dashed) and after (solid) the addition of 0.25 mM EDTA. (B) CVs of 1 mM Co-TDMImP (red) and 0.2 mM $Co(NO_3)_2$ (black) before (dashed) and 10 minutes after (solid) the addition of 0.5 g Chelex resin. Other conditions: room temperature, 0.2 M Na-Pi buffer, pH 7, scan rate 100 mV s^{-1}.

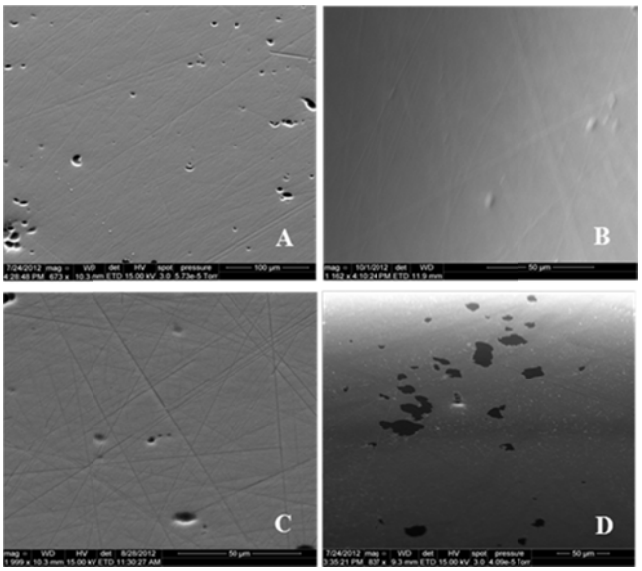

Figure S12. ESEM images of (A) freshly polished glassy carbon electrode; (B) glassy carbon electrode after 20 CV scans in 0.2 M Na-Pi pH 7 solution containing 5 mM Co-TDMImP; and a cobalt oxide film on a glassy carbon electrode after 20 CV scans in the same buffer containing (C) 0.1 mM and (D) 1 mM $Co(NO_3)_2$.

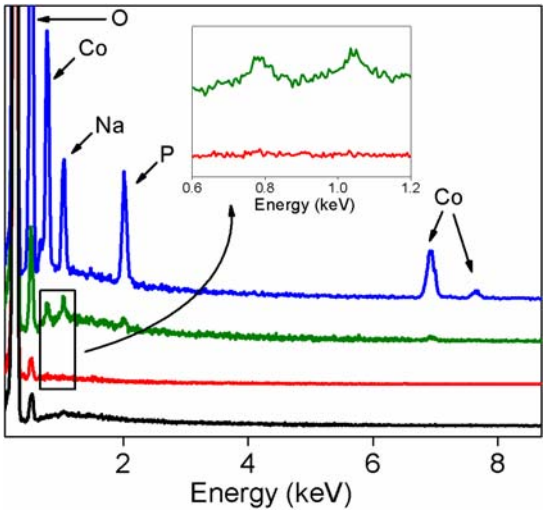

Figure S13. EDX analysis of freshly polished glassy carbon electrode (blake); glassy carbon electrode after 20 CV scans in 0.2 M Na-Pi pH 7 solution containing 5 mM Co-TDMImP (red); and a cobalt oxide film on a glassy carbon electrode after 20 CV scans in the same buffer containing 0.1 mM (green) and 1 mM $Co(NO_3)_2$ (blue).

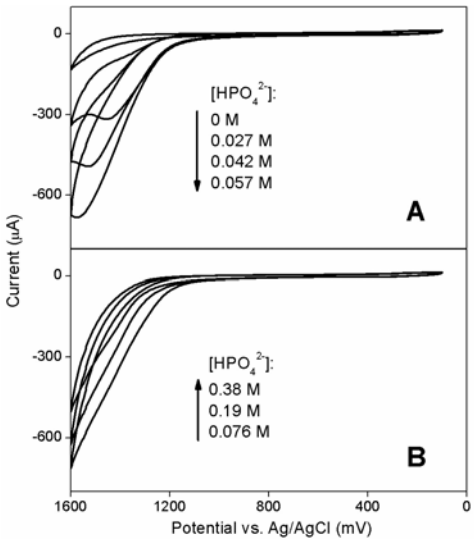

Figure S14. CVs of 1 mM Co-TDMImP at room temperature and a scan rate of 100 mV s^{-1} in pH 7 Na-Pi buffer solutions at HPO_4^{2-} concentration of (panel A, from top to bottom) 0 M, 0.027 M, 0.042 M, 0.057 M, and (panel B, from bottom to top) 0.076 M, 0.19 M and 0.38 M. Standard deviations for these curves are in a range of ±20 μA and were shown in Figure 2A.

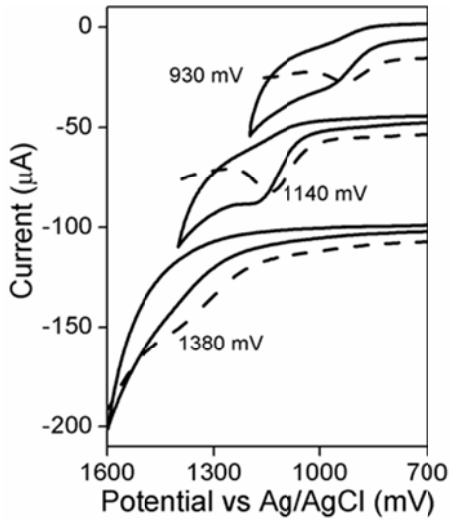

Figure S15. CVs (solid lines) and SWVs (dashed lines) of (from top to bottom) 1 mM Ga^{III}-TTMAP, Ga^{III}-TM4PyP and Ga^{III}-TDMImP. Peak potentials are labeled. Other conditions: room temperature, scan rate 100 mV s^{-1}, 0.2 M Na-Pi buffer, pH 7.

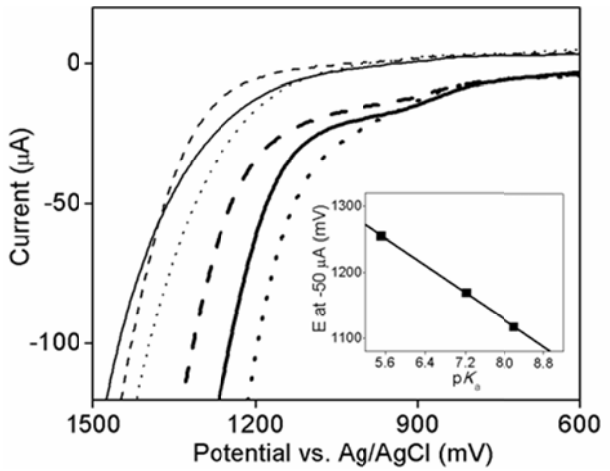

Figure S16. CVs of 1 mM Co-TTMAP at room temperature and a scan rate of 100 mV s^{-1} at pH 7 in phthalate (dashed), Na-Pi (solid) and *n*-butylphosphonate (dotted) buffers. Inset: Plot of the potential measured at -50 μA as a function of pK_a of the buffer species. The red line represents the best linear fit with a slope of -50 mV pK_a^{-1}.

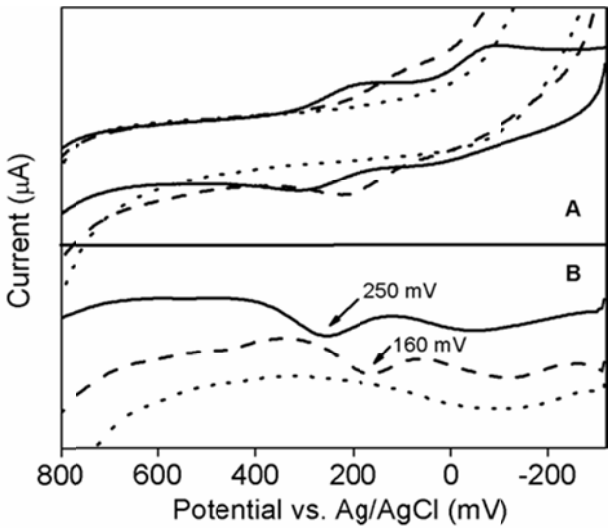

Figure S17. CVs (panel A) and SWVs (panel B) of 1 mM Co-TDMImP (solid), Co-TM4PyP (dashed) and Co-TTMAP (dotted). Other conditions: room temperature, scan rate 100 mV s^{-1}, 0.2 M Na-Pi buffer, pH 7. The $Co^{III/II}$ potentials for Co-TDMImP and Co-TM4PyP are labeled.

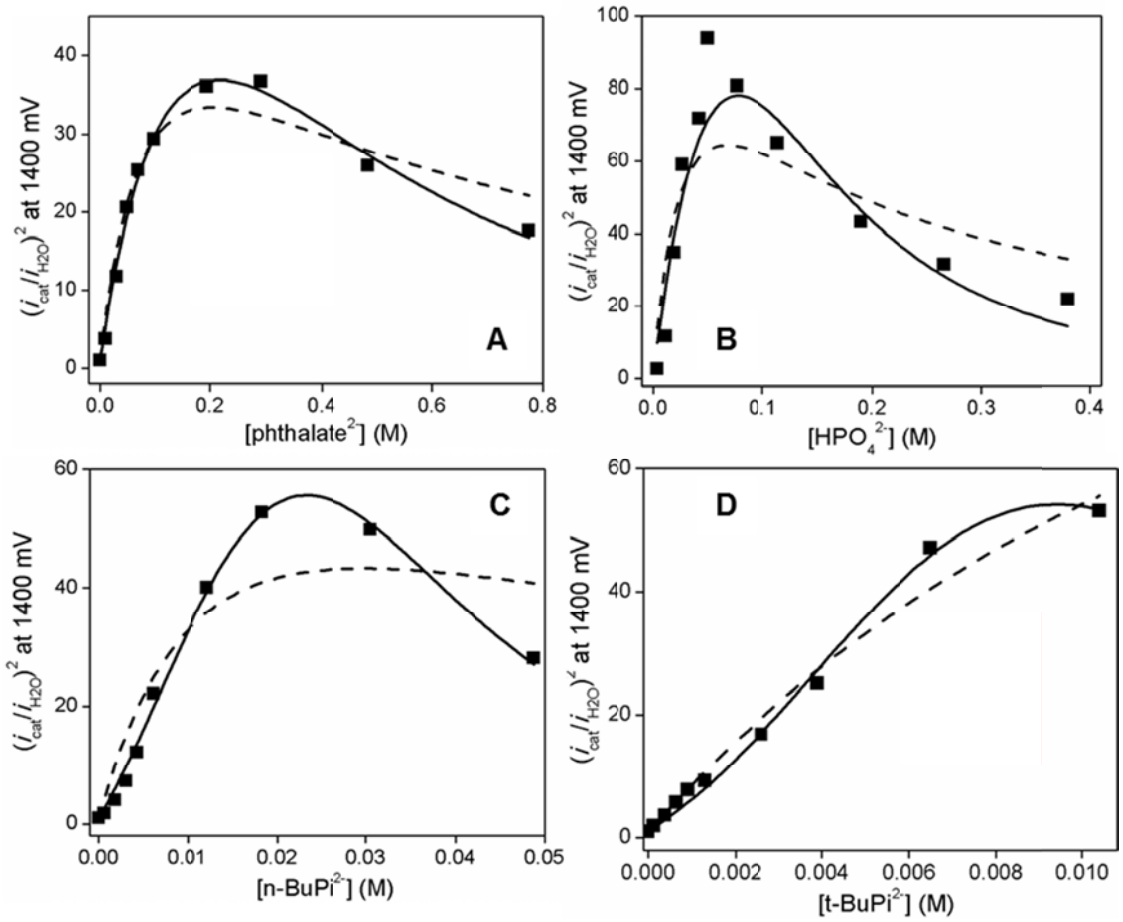

Figure S18. Experimental (filled black squares) and fitted (curves) results of $(i_{cat}/i_{water})^2$ as a function of buffer dianion concentration for (A) phthalate, (B) Na-Pi, (C) *n*-butylphosphonate and (D) *t*-butylphosphonate. Solid curves represent the best fits using eq. S3. Dashed curves represent fits assuming that there is no formation of the doubly bound species Co^{III}-B_2 ($K_{eq,2}$ = 0).

1. Tjahjono DH, Akutsu T, Yoshioka N, & Inoue H (1999) Cationic porphyrins bearing diazolium rings: synthesis and their interaction with calf thymus DNA. *Biochim Biophys Acta* 1472(1-2):333-343.
2. Kachadouriana R, Johnson CA, Mina E, Spasojevic I, & Day BJ (2004) Flavin-dependent antioxidant properties of a new series of meso-N,N'-dialkyl-imidazolium substituted manganese(III) porphyrins. *Biochemical Pharmacology* 67(1):77-85.
3. Batinic-Haberle I, Benov L, Spasojevic I, & Fridovich I (1998) The ortho effect makes manganese(III) meso-tetrakis-(N-methylpyridinium-2-yl)porphyrin a powerful and potentially useful superoxide dismutase mimic. *J Biol Chem* 273(38):24521-24528.